Mineralogy and Petrology (2018) 112 (Suppl 2):S539–S554
https://doi.org/10.1007/s00710-018-0607-6

ORIGINAL PAPER

Origin of complex zoning in olivine from diverse, diamondiferous kimberlites and tectonic settings: Ekati (Canada), Alto Paranaiba (Brazil) and Kaalvallei (South Africa)

Emilie Lim[1] · Andrea Giuliani[1,2] · David Phillips[1] · Karsten Goemann[3]

Received: 2 December 2017 / Accepted: 12 June 2018 / Published online: 6 July 2018

Abstract

Olivine in kimberlites can provide unique insights into magma petrogenesis, because it is the most abundant xenocrystic phase and a stable magmatic product over most of the liquid line of descent. In this study we examined the petrography and chemistry of olivine in kimberlites from different tectonic settings, including the Slave craton, Canada (Ekati: Grizzly, Koala), the Brasilia mobile belt (Limpeza-18, Tres Ranchos-04), and the Kaapvaal craton, South Africa (Kaalvallei: Samada, New Robinson). Olivine cores display a wide range of compositions (e.g., Mg# = 78–95). The similarity in olivine composition, resorption of core zones and inclusions of mantle-derived phases, indicates that most olivine cores originated from the disaggregation of mantle peridotites, including kimberlite-metasomatised lithologies (i.e. sheared lherzolites and megacrysts). Olivine rims typically show a restricted range of Mg#, with decreasing Ni and increasing Mn and Ca contents, a characteristic of kimberlitic olivine worldwide. The rims host inclusions of groundmass minerals, which implies crystallisation just before and/or during emplacement. There is a direct correlation between olivine rim composition and groundmass mineralogy, whereby high Mg/Fe rims are associated with carbonate-rich kimberlites, and lower Mg/Fe rims are correlated with increased phlogopite and Fe-bearing oxide mineral abundances. There are no differences in olivine composition between explosive (Grizzly) and hypabyssal (Koala) kimberlites. Olivine in kimberlites also displays *transitional zones* and less common *internal zones*, between cores and rims. The diffuse transitional zones exhibit intermediate compositions between cores and rims, attributed to partial re-equilibration of xenocrystic cores with the ascending kimberlite melt. In contrast, internal zones form discrete layers with resorbed margins and restricted Mg# values, but variable Ni, Mn and Ca concentrations, which indicates a discrete crystallization event from precursor kimberlite melts at mantle depths. Overall, olivine exhibits broadly analogous zoning in kimberlites worldwide. Variable compositions for individual zones relate to different parental melt compositions rather than variations in tectonic setting or emplacement mechanism.

Keywords Kimberlite · Olivine · Zoning

Editorial handling: P. Janney

Electronic supplementary material The online version of this article (https://doi.org/10.1007/s00710-018-0607-6) contains supplementary material, which is available to authorized users.

✉ Andrea Giuliani
andrea.giuliani@unimelb.edu.au; andrea.giuliani@mq.edu.au

[1] KiDs (Kimberlites and Diamonds), School of Earth Sciences, University of Melbourne, Parkville, VIC 3010, Australia

[2] Australian Research Council Centre of Excellence for Core to Crust Fluid Systems (CCFS) and National Key Centre for Geochemical Evolution and Metallogeny of Continents (GEMOC), Department of Earth and Planetary Sciences, Macquarie University, North Ryde, NSW 2109, Australia

[3] Central Science Laboratory, University of Tasmania, Hobart, TAS 7001, Australia

Introduction

Olivine is the most abundant phase in coherent kimberlites, typically accounting for 40 to 60% of rock volumes (e.g., Brett et al. 2009; Moss et al. 2010; Soltys et al. 2018a). Olivine is a primary liquidus phase in kimberlite melts (e.g., Mitchell 2008) and crystallises throughout most of the crystallisation sequence, as indicated by inclusions of groundmass phases in olivine rims (e.g., Bussweiler et al. 2015; Kamenetsky et al. 2008; Giuliani et al. 2017; Soltys et al. 2018b). In addition, olivine is the most abundant xenocrystic component in kimberlites, with volumetric contents estimated at ~20 to 50% (Brett et al. 2009; Fedortchouk and Canil 2004; Bussweiler et al. 2015). Since there is also abundant evidence of interaction between kimberlites and entrained mantle wall

rocks (Canil and Fedortchouk 1999; Cordier et al. 2015; Hunter and Taylor 1982; Mitchell 2008; Kamenetsky et al. 2009, 2014a; Russell et al. 2012; Soltys et al. 2016), studies of olivine provide the opportunity to deconvolve the evolution of kimberlite melts.

Olivine grains in kimberlites worldwide generally contain a xenocrystic core overgrown by one or more texturally and/or compositionally distinct zones (Brett et al. 2009; Bussweiler et al. 2015; Fedortchouk and Canil 2004; Giuliani 2018; Giuliani et al. 2017; Howarth and Taylor 2016; Nielsen and Sand 2008; Sazonova et al. 2015; Shaikh et al. 2018; Sobolev et al. 2015; Soltys et al. 2018b). These zones have been defined using different terminology in the literature. To avoid confusion, the terms employed in this article are defined as follows. The *core* is defined as the central, compositionally distinct zone observed in most olivine grains. *Rim* is defined as the magmatic overgrowth that is common to olivine in most kimberlites and is equivalent to the 'margins' or 'melt zones' described in some publications. *Rind* is the magmatic zone that fringes the olivine rims in some (fresh) kimberlites. There is general consensus that the rims and rinds have a magmatic origin, with the cores originating from disaggregated mantle rocks. However, considerable debate remains regarding the following aspects of olivine compositions and their formation:

1) There is increasing evidence that part of the olivine core population originated from peridotite modified by precursor kimberlite melts (Arndt et al. 2010; Giuliani 2018; Howarth and Taylor 2016; Sazonova et al. 2015; Sobolev et al. 2015). The exact nature of the source peridotite is uncertain and suggestions range from 'defertilised' dunites (Arndt et al. 2010) to metasomatised lherzolites (Sobolev et al. 2015) and Cr-rich megacrysts (Moore and Costin 2016).
2) There is uncertainty relating to the mechanism(s) that generate olivine rims with almost constant Mg#, but variable Ni, Mn and Ca contents. Explanations range from atypical element partition coefficients between olivine and kimberlite melts (Cordier et al. 2015; Kamenetsky et al. 2008), to fractional crystallisation of olivine and oxide minerals during digestion of orthopyroxene xenocrysts (Pilbeam et al. 2013).
3) The origin of intermediate zones between cores and rims in kimberlitic olivine is poorly constrained. Suggested causative mechanisms include kimberlite-related 'dunitisation' of the magmatic conduit (Cordier et al. 2015), multiple dissolution and overgrowth events (Sobolev et al. 2015), and partial core re-equilibration with the host kimberlite magma (Howarth and Taylor 2016).

In addition, previous studies have established that magmatic olivine in global kimberlites have a restricted range in composition, with Mg# [100 × Mg/(Mg + Fe)] ratios of ~88–91 (e.g., Brett et al. 2009; Bussweiler et al. 2015; Fedortchouk and Canil 2004; Giuliani 2018; Kamenetsky et al. 2008; Nielsen and Sand 2008; Shaikh et al. 2018). This observation seems at variance with the variable groundmass mineralogy of worldwide kimberlites, ranging from those dominated by carbonates (e.g., Armstrong et al. 2004) to phlogopite-rich examples (e.g., Downes et al. 2006; Taylor and Kingdom 1999). To address the potential correlation between olivine and groundmass composition, and provide new constraints on the origin of olivine zoning, we have examined the petrography and olivine major-element chemistry of diamond-bearing kimberlites from a diversity of localities: Grizzly and Koala (Ekati property), Lac de Gras, Canada; Limpeza-18 and Tres Ranchos-04, Alto Paranaiba Igneous Province, Brazil; Samada and New Robinson (Kaalvallei cluster), South Africa (Fig. 1). This is the first detailed study of olivine in Brazilian kimberlites. The examined kimberlites were emplaced in different tectonic settings and exhibit variable textures and groundmass compositions, as well as different olivine characteristics. This unique dataset provides new insights into the origin of olivine compositional variations and the evolution of kimberlite magmas.

Samples

The Grizzly and Koala kimberlites are located in the Lac de Gras kimberlite field of the Slave craton, Canada. The studied samples derive from holes drilled by BHP during preliminary investigations of these pipes. The Grizzly pipe contains coherent magmatic kimberlite of likely pyroclastic origin (Nowicki et al. 2008; Webb et al. 2008). The Koala pipe hosts a layered sequence of volcanoclastic kimberlite units, which overlies a basal unit ('P7') of hypabyssal kimberlite (Nowicki et al. 2004; Porritt and Cas 2011), the source of the Koala sample.

The Limpeza-18 and Tres Ranchos-04 kimberlites form part of a widespread province of kimberlites, kamafugites and other alkaline rocks, the Alto Paranaiba Igneous Province, within the Late Cambrian Brasilia Belt, along the margin of the Sao Francisco craton (Araujo et al. 2001; Felgate 2014; Gibson et al. 1995; Guarino et al. 2013). Representative samples from Limpeza-18 (407/409/0036/1) and Tres Ranchos-04 (407/409/004/6) were obtained from the De Beers collection.

Samada and New Robinson are two of the three pipes that comprise the Kaalvallei cluster, which intruded into the Kaapvaal craton, South Africa. The Samada sample (173/44/K8/7) is from the De Beers collection, whereas the New Robinson sample (JJG-2828) was sourced in the John J. Gurney Upper Mantle Room Collection, University of Cape Town.

Fig. 1 Locality map showing the distribution of kimberlites examined in this study. Red circles represent locations of kimberlites

Analytical methods

Sample textures and petrography were first characterised under transmitted and reflected light using a Leica DM750P microscope. The study of microstructures, mineral inclusions and olivine zoning was performed using a Phillips FEI XL30 environmental scanning electron microscope (ESEM) equipped with an OXFORD INCA energy-dispersive X-ray spectrometer (EDS), and a Hitachi SU-70 field emission scanning electron microscope (FE-SEM) equipped with an OXFORD AZtec-XMax80 EDS. The relative abundances of mineral phases in the groundmass were calculated using BSE images and the image-analysis software JMicroVision 1.2.7 (https://www.jmicrovision.com/).

Different compositional zones of each olivine grain (e.g., cores, rims) were identified using BSE images. Major and minor oxide concentrations were then measured using a Cameca SX50 electron probe micro-analyser (EPMA), with some analyses performed with a Cameca SX100 EPMA. Analytical conditions were as follows: beam current of 25 or 35 nA, beam accelerating voltage of 15 kV, and beam diameter of 1–2 μm; counting times of 20–40 s on peak positions and 10–40 s on two background positions located on either side of the peak position. Both natural (e.g., Durango apatite) and synthetic materials (e.g., synthetic periclase from the University of Melbourne) were used for calibration purposes. All elements analysed monitored the k-alpha X-ray lines except for Nb (l-alpha), and data reduction was carried out using the PAP matrix correction software program.

Petrography

Grizzly

The Grizzly kimberlite, as well as the other examined samples, exhibits a typical porphyritic texture (Fig. 2) with variable quantities of olivine macrocrysts (rounded or anhedral grains, larger than 0.5–1.0 mm), phenocrysts (euhedral to subhedral crystals, >0.5 mm in size) and micro-phenocrysts (<0.5 mm). Dunite micro-xenoliths (polygranular 'nodules' of Arndt et al. 2010) have been observed in some samples, including Grizzly.

The majority of small (<0.5 mm) olivine grains in the Grizzly kimberlite show angular shapes indicating explosive emplacement (Fig. 2a). Olivine grains are fresh, with only minimal alteration to serpentine and carbonates along the grain edges and fractures. Olivine grains are zoned and typically consist of a core, rim and internal zone between core and rim (Fig. 3a). Cores are generally rounded or show embayments, probably due to resorption. Olivine internal zones are ≤40 μm thick, while rims can be up to 150 μm wide. Olivine grains devoid of compositional zoning are rare. The most

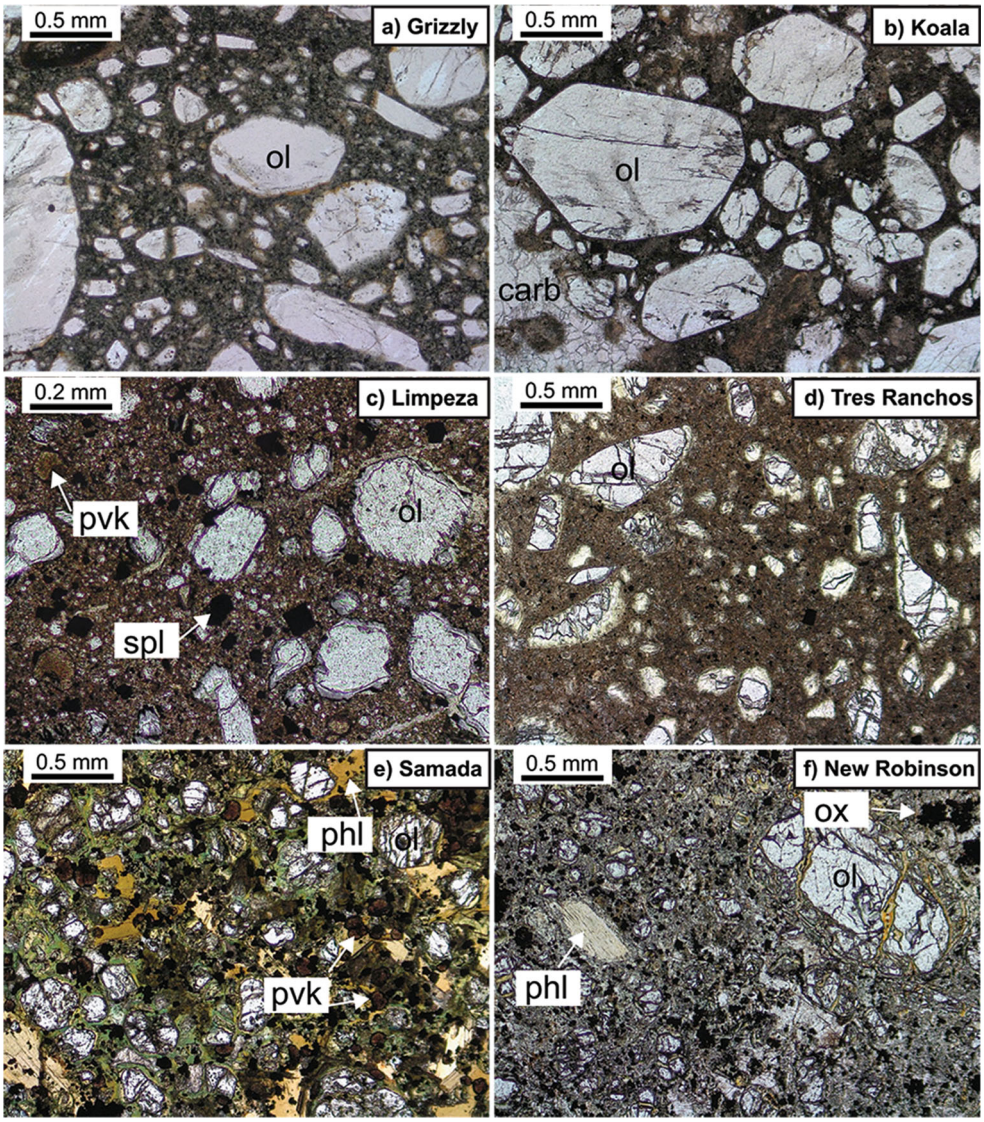

Fig. 2 Optical photomicrographs (plane-polarised light) showing the texture and olivine morphologies of kimberlites from (**a**) Grizzly, (**b**) Koala, (**c**) Limpeza 18, (**d**) Tres Ranchos 4, (**e**) Samada, and (**f**) New Robinson. Note the angular and shard-like shapes of olivine grains in the Grizzly and Tres Ranchos 4 kimberlites. ol = olivine, carb = carbonates, pvk = perovskite, spl = spinel, phl = phlogopite, ox = oxides

common inclusion in olivine is spinel; i.e. Cr-spinel in the cores and magnesio-ulvöspinel-magnetite (MUM) in the rims.

The sample also contains occasional phlogopite and garnet macrocrysts. In addition, kinoshitalite mica occurs as rare, 200–400 μm long, poikilitic phenocrysts with monticellite and spinel inclusions (Fig. 4a). The groundmass includes (in order of decreasing abundance) monticellite, carbonates, serpentine, spinel-group minerals, phlogopite, apatite, perovskite, minor barite and sulfides (Table 1). Carbonates are mostly calcite with lesser dolomite and, together with serpentine, occur as an interstitial mesostasis. Country rock xenoliths observed (< 2 vol%) are completely altered to mixtures of fine-grained minerals.

Koala

In contrast to the Grizzly kimberlite, olivine in our Koala sample forms (not fragmented) euhedral to subhedral crystals, regardless of size (<0.1–5 mm; Fig. 2b). Olivine is very fresh with only minimal alteration to serpentine. The majority of olivine grains are zoned and include core, rim, and multiple rinds (up to ~30), each a few μm thick (Fig. 3b). Rims and rinds form composite overgrowths around cores, up to 300 μm thick. Inclusions of Cr-spinel and Cr-diopside are present in olivine cores. Spinel inclusions (chromite to MUM) occur in the rims, whereas MUM spinel, phlogopite and calcite are included in rinds (see also Kamenetsky et al. 2013).

Olivine, calcite ± dolomite aggregates (segregations) and occasional phlogopite macrocrysts are in a groundmass consisting of carbonates, serpentine, spinel, phlogopite, apatite and monticellite (Fig. 4b; Table 1). Monticellite is largely pseudomorphed by serpentine, although its characteristic rounded euhedral shape is still apparent (Fig. 4b). Spinel grains commonly show atoll shapes with cores zoned from chromite to MUM, and pleonaste occasionally preserved in the lagoon between chromite-MUM and magnetite rims. No

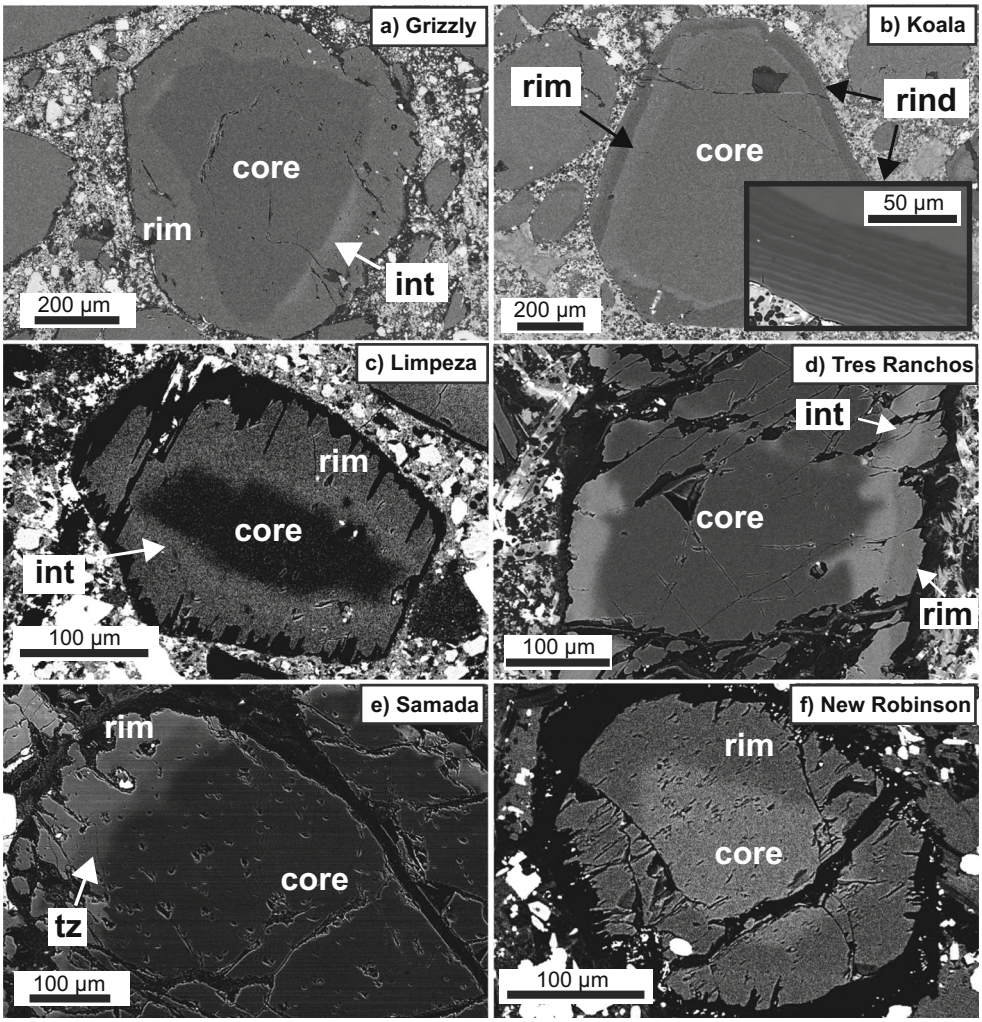

Fig. 3 BSE images of representative, zoned olivine grains from (**a**) Grizzly, (**b**) Koala, (**c**) Limpeza 18, (**d**) Tres Ranchos 4, (**e**) Samada, and (**f**) New Robinson. Note the internal zone ('int') between core and rim in grains from Grizzly, Limpeza 18 and Tres Ranchos 4; the finely layered rind of Koala olivine; and the diffuse transitional zone ('tz') between core and rim in Samada olivine

perovskite was observed, whereas trace amounts of sulfides (djerfisherite and pyrite), pyrochlore [$(Na,Ca)_2Nb_2O_6(OH,F)$] and priderite [$K(Ti_7Fe^{3+})O_{16}$] occur in the groundmass. Altered country rock material is rare (< 3 vol%).

Limpeza-18

In contrast to the Ekati kimberlites, the Limpeza-18 sample contains more abundant olivine phenocrysts and micro-phenocrysts (65%) than macrocrysts (Fig. 2c). Internal zones are occasionally observed between cores and rim (Fig. 3c). Olivine rims host inclusions of MUM spinel, chromite, apatite, phlogopite and perovskite. Dunite micro-xenoliths (~1 mm) were also observed in this sample.

Monticellite is the major groundmass constituent and occurs as small crystals (<40 µm and occasionally up to ~100 µm in size). Phlogopite micro-phenocrysts, 100–200 µm in size, are relatively common. Other major groundmass components include spinel (chromite to MUM; <50 µm); perovskite (up to 200 µm, but generally <100 µm), which contains inclusions of spinel; apatite often intergrown with phlogopite (Fig. 4c); and interstitial serpentine. Carbonates are notably absent in this sample. We speculate this might be due to immiscible separation and removal of a carbonate melt rather than complete CO_2 degassing, which commonly produces pyroclastic kimberlites without primary carbonates.

Tres Ranchos-04

Similar to the Grizzly kimberlite, the majority of olivine grains in the Tres Ranchos-04 kimberlite show angular and shard-like shapes (Fig. 2d), which indicates moderately explosive emplacement of the parental magma. Euhedral to subhedral phenocrysts are only occasionally observed. In contrast to Limpeza-18, olivine macrocrysts are significantly more abundant than (micro-)phenocrysts. Olivine is zoned with common internal zones between cores and rims (Figs. 3d and 5a). Unzoned grains are again rare.

The macrocryst population of the Tres Ranchos-04 kimberlite includes Cr-diopside, Cr-spinel and abundant phlogopite. The groundmass consists of carbonates (calcite and lesser

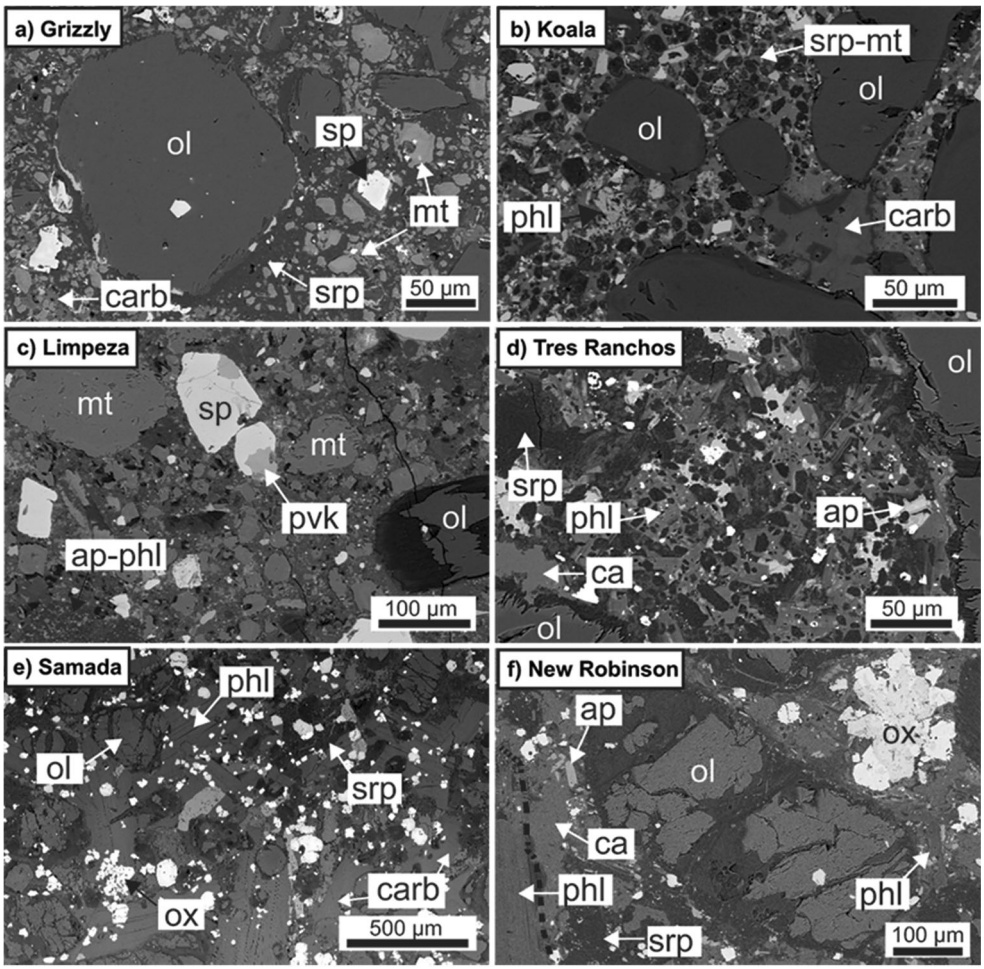

Fig. 4 BSE images showing the main groundmass features of examined kimberlites: (**a**) Grizzly, (**b**) Koala, (**c**) Limpeza 18, (**d**) Tres Ranchos 4, (**e**) Samada, and (**f**) New Robinson. For the Ekati kimberlites (a, b), note the enrichment in carbonates ('carb') and monticellite ('mt'), which is largely serpentinised ('srp-mt') in Koala. The Limpeza groundmass is dominated by fresh monticellite. Phlogopite ('phl') and oxide minerals (spinel + Mg-ilmenite; 'ox') are very abundant in the groundmass of the Kaalvallei kimberlites (e, f). ol = olivine, sp. = spinel, pvk = perovskite, ap = apatite, srp = serpentine, ca = calcite

dolomite), mica (intermediate between phlogopite and kinoshitalite), serpentine, spinel, apatite, perovskite and barite (Fig. 4d; Table 1) and can be separated into domains enriched in carbonates or phlogopite. Monticellite is largely replaced by serpentine. Groundmass spinel is mainly MUM with occasional chromite cores, whereas some larger (>100 μm) grains contain Al-rich cores [Cr/(Cr + Al) < 0.50]. Apatite is abundant and displays a dendritic texture with Sr-rich cores in the carbonate-rich domains (Supplementary Fig. S1). Barite is relatively abundant in the groundmass, especially in the carbonate-rich domains, and occurs together with apatite as inclusions in calcite.

Samada

The Samada sample is unusual in that it contains a relatively coarse-grained groundmass (>50 μm; Fig. 2e). Olivine is again the major constituent, comprising ~40 vol% of the rock. Olivine is more serpentinised than in the other kimberlites with most micro-phenocrysts being extensively altered. Olivine zoning includes cores, rims, rinds (Supplementary Fig. S1), and diffuse layers between cores and rims (transitional zones; Fig. 3e, and Supplementary Fig. S2). A characteristic feature of the Samada olivine is the widespread occurrence of ilmenite inclusions, which are <10 μm in size, typically rounded, and often form a 'necklace' within the olivine rim (Fig. S1; see also Stiefenhofer 1989).

The groundmass consists of serpentine, phlogopite, spinel, Mg-ilmenite, carbonates, perovskite and apatite (Fig. 4e). Phlogopite occurs interstitial to olivine and hosts abundant inclusions of oxide minerals. Clusters of oxide phases are common, and often exhibit Mg-ilmenite cores mantled by MUM spinel, Ti-magnetite and perovskite. Intergrowths of perovskite and MUM spinel were also observed occasionally. The small number of crustal xenocrysts present (~1–2 vol%) are all altered.

New Robinson

Olivine macrocrysts and (micro-)phenocrysts in this kimberlite are pervasively fractured with serpentinisation along margins and fractures (Fig. 2f). The majority of olivine grains are, however, euhedral to rounded in shape. Macrocrysts and (micro-)phenocrysts occur in similar proportions. Olivine

Table 1 Estimated abundance of groundmass components (normalised to 100 vol% on an olivine-free basis) and kimberlite classification

Kimberlite	Locality		Textural classification	Estimated proportions of groundmass minerals, excluding olivine (%)							Petrographic classification
				Carbonates	Monticellite	Phlogopite	Spinel + ilmenite	Perovskite	Apatite	Serpentine	
Grizzly	Ekati Property, Lac de Gras, Canada		Pipe-filling coherent	11	37	3	6	3	7	33	Carbonate-serpentine-monticellite kimberlite
Koala	Ekati Property, Lac de Gras, Canada		Hypabyssal	51	Altered to serpentine (18)	6	6	Not observed	3	16	Monticellite-serpentine-carbonate kimberlite
Limpeza 18	South Brazilia fold belt, Goias State, Brazil		Hypabyssal	Not observed	31	24	8	6	12	19	Phlogopite monticellite kimberlite
Tres Ranchos 4	South Brazilia fold belt, Goias State, Brazil		Pipe-filling coherent	24	Altered to serpentine (4)	24	3	3	14	30	Phlogopite carbonate-serpentine kimberlite
Samada	Kaalvallei cluster, Kaapvaal, South Africa		Hypabyssal	10	Altered to serpentine	27	15	7	2	41	Oxide-rich phlogopite-serpentine kimberlite
New Robinson	Kaalvallei cluster, Kaapvaal, South Africa		Hypabyssal	22	Altered to serpentine	28	13	3	6	29	Oxide-rich calcite-phlogopite-serpentine kimberlite

typically shows simple concentric zoning with a core and a rim, often separated by a diffuse transitional zone (Figs. 3f and 5c, and Supplementary Fig. S2). The most common inclusions in the rims are Mg-ilmenite (Fig. S1), with lesser MUM spinel and phlogopite.

Olivine, abundant phlogopite macrocrysts and (micro-)phenocrysts, plus large (>1 mm) ilmenite macrocrysts occur in a groundmass composed of serpentine, phlogopite, calcite, oxide minerals (Mg-ilmenite, MUM spinel, Ti-magnetite, perovskite and minor chromite), and apatite (Fig. 4f). Monomineralic calcite aggregates and ≤ 400 μm clusters of oxide minerals are common (Fig. S1). Trace amounts of sulfides (e.g., pyrite) are also present in the groundmass.

Olivine chemistry

The major and minor element compositions of different olivine zones for each sample are plotted in Figs. 6, 7, 8, 9, 10 and 11, with the complete dataset reported in Supplementary Tables. Two types of core composition are distinguished based on Mg#, Ni, Mn and Ca contents, namely 'Mg-rich (Mg# >89) and 'Fe-rich' cores (Mg# <89). Compositions of rims, rinds, internal and transitional zones are plotted using different symbols.

Grizzly

Thirty-five olivine grains were analysed in the Grizzly sample (Fig. 6). The cores show Mg# ranging from 89.8 to 94.1, with high NiO (0.26–0.45 wt%), variable MnO (0.03–0.19 wt%) and low CaO (< 0.09 wt%) contents. Olivine internal zones ($n = 4$) are characterised by modest variations in Mg# (90.2–90.8) and NiO (0.25–0.30 wt%). The rims show a relatively constant Mg# (90.7–92.0), with decreasing NiO (0.44–0.07 wt%) and increasing MnO (0.09–0.23 wt%) and CaO (0.02–0.38 wt%) contents (see also Fedortchouk and Canil 2004). A single olivine grain contains a rind with high Mg# (92.4), low NiO (0.03 wt%), high MnO (0.31 wt%) and CaO (0.45 wt%) concentrations. Two unzoned grains yielded compositions typical of cores and rims, respectively.

Koala

The compositions of 33 olivine grains from the Koala sample were measured (Fig. 7). The majority of the cores have Mg# values overlapping those of Grizzly olivine (89.9–93.1; 'Mg-rich cores'), with four grains exhibiting lower Mg# (85.3–88.9) and higher MnO contents (0.16–0.20 wt%; 'Fe-rich cores'). Olivine rims are characterised by constant Mg# (90.8–91.8), decreasing NiO (0.32 to 0.14 wt%) and increasing MnO (0.10–0.23 wt%) and CaO (0.04–0.16 wt%) contents. Transitional zones show intermediate compositions

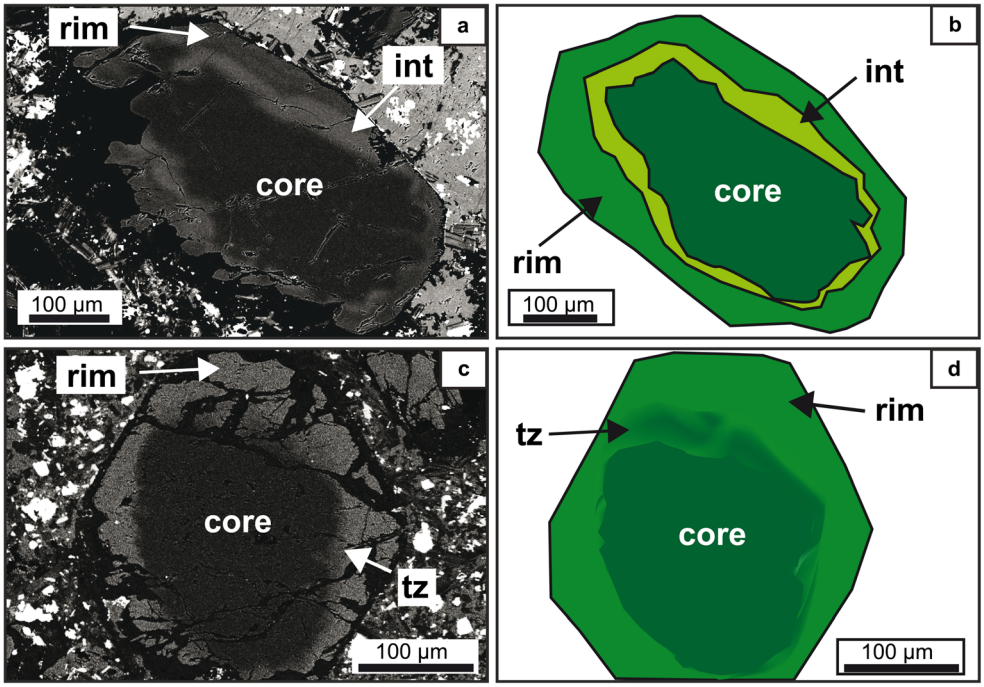

Fig. 5 BSE images and schematic diagrams of complexly zoned olivine grains from (**a**, **b**) Tres Ranchos-04, and (**c**, **d**) New Robinson. These grains were selected because they contain well defined internal (a, b) and transitional zones (c, d), respectively

between cores and rims (e.g., Mg# = 90.5–92.7; n = 4). Individual zones in the olivine rinds (Fig. 3b) could not be measured due to their limited thickness (<5 µm). Overall the rinds form an array trending from the rim compositions towards increasing Mg# (from 92.1 to 95.0), MnO (0.19–0.34 wt%) and CaO (0.12 to 0.56 wt%), and decreasing NiO concentrations (0.17 to 0.05 wt%; Fig. 7). One unzoned olivine grain lies within the field of mantle core compositions.

Limpeza-18

The 32 olivine grains measured in this kimberlite contain either 'Mg-rich' (Mg# = 89–92; NiO = 0.34–0.46 wt%; CaO < 0.12 wt%; $n = 16$) or 'Fe-rich' cores (Mg# = 83–88; NiO = 0.22–0.42 wt%; CaO = 0.07–0.14 wt% with an outlier at 0.02 wt%; n = 16; Fig. 8). Nickel and Mn concentrations in the Fe-rich cores show broadly direct and inverse correlations with Mg#, respectively. Internal zones ($n = 5$) have a constant Mg# of 84.1 ± 0.3 (1 s.d.) with variable NiO (0.19–0.31 wt%) and CaO concentrations (0.08–0.14 wt%), at constant MnO (0.17–0.19 wt%). The rims exhibit higher Mg# value (85–87) than the internal zones. The rim NiO contents decrease from 0.38 to 0.06 wt% while MnO and CaO both increase (0.15–0.28 wt% and 0.07–0.40 wt%, respectively).

Tres Ranchos-04

Thirty-two olivine grains were measured in the Tres Ranchos-04 sample (Fig. 9). In contrast to Limpeza-18, the majority of cores show high Mg# (90–93), NiO (0.33–0.43 wt%), moderate MnO (0.04–0.18 wt%), and low CaO concentrations (<

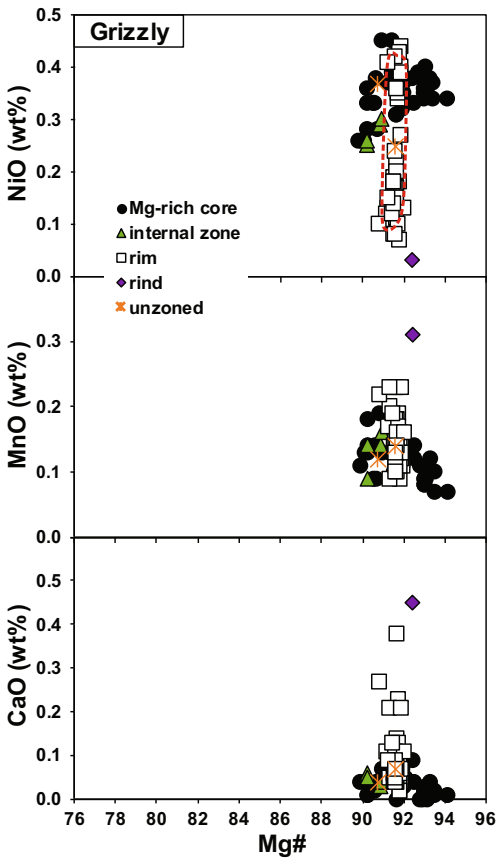

Fig. 6 Mg# vs NiO, MnO and CaO covariations charts of different zones in olivine grains from the Grizzly kimberlite pipe (Ekati property), Lac de Gras, Canada. The red shape in the upper panel indicates the composition of olivine rims in other samples of the Grizzly kimberlite measured by Fedortchouk and Canil (2004)

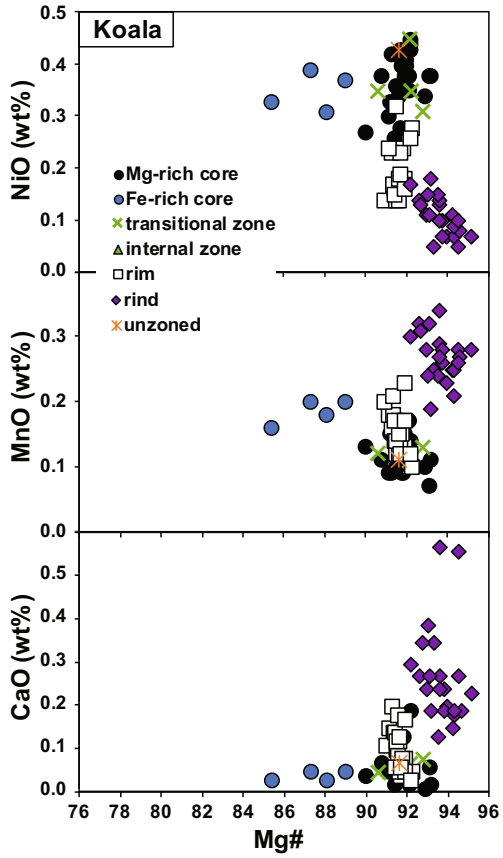

Fig. 7 Mg# vs NiO, MnO and CaO covariations charts of different zones in olivine grains from the basal hypabyssal unit of the Koala kimberlite pipe (Ekati property), Lac de Gras, Canada

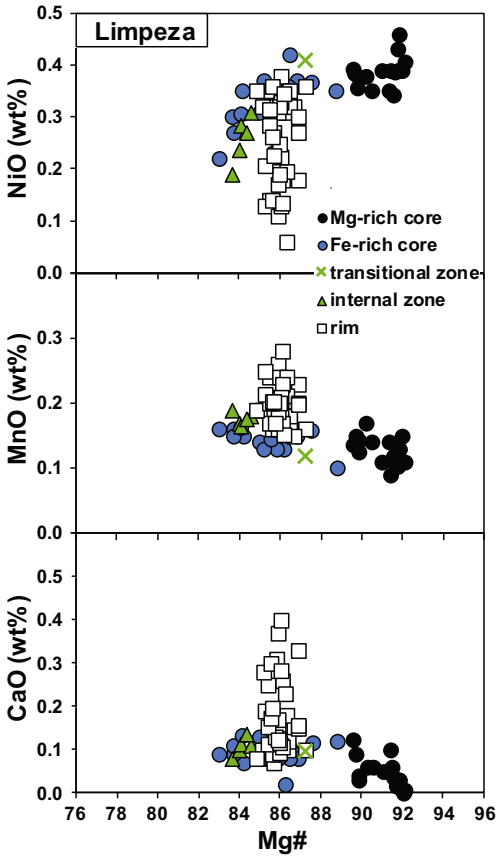

Fig. 8 Mg# vs NiO, MnO and CaO covariations charts of different zones in olivine grains from the Limpeza-18 kimberlite, Alto Paranaiba Igneous Province, Brazil

0.05 wt%; 'Mg-rich' cores). Two 'Fe-rich' cores are distinguished by lower Mg# values of 85.0 and 87.1. The internal zones have relatively constant Mg# (87.0–88.4), and similar NiO, CaO and MnO to the rims. As for the other kimberlites, the rims show a restricted range of Mg# values (88.8–90.0), decreasing NiO (0.41–0.14 wt%) and increasing MnO (0.10–0.29 wt%) and CaO contents (0.03–0.16 wt%). Three unzoned grains were analysed and show compositions similar to Fe-rich (2) and Mg-rich cores (1).

Samada

Of the 29 olivine grains analysed in the Samada sample, 6 cores are classified as 'Mg-rich' based on their high Mg# values (92.0–93.4) and NiO contents (0.37–0.41 wt%) coupled with moderately low MnO (0.09–0.11 wt%) and CaO concentrations (0.04–0.11 wt%; Fig. 10). The 23 'Fe-rich' cores have lower Mg# (78.2–88.9) than the 'Mg-rich' cores, with NiO (0.03–0.40 wt%) and MnO contents (0.09–0.22 wt%) directly, and inversely, correlated to Mg#, respectively. Additional core compositions measured by Stiefenhofer (1989; $n = 18$) belong to the Fe-rich group, with a single exception (Fig. 10). The rim compositions show constant Mg# (84.5 ± 0.3, 1 s.d., $n = 11$), decreasing NiO (0.24–0.09 wt%), and increasing CaO concentrations (0.13–0.20 wt%). Some olivine grains exhibit rinds with higher Mg# (85.0–87.0), MnO (0.21–0.26 wt%) and CaO (0.35–0.54 wt%), and lower NiO abundances (0.08–0.12 wt%) than the rims. Transitional zones between cores and rims have a wide compositional range (e.g., Mg# = 83.2–89.2) intermediate between core and rim values. Two analyses show CaO concentrations greater than those of olivine cores and rims, which might be due to minor carbonate contamination.

New Robinson

Analyses were conducted on 21 olivine grains from the New Robinson kimberlite (Fig. 11). Similar to Samada, 'Mg-rich' cores (Mg# = 91.3–94.9; NiO = 0.36–0.47 wt%; CaO < 0.04 wt%; $n = 5$) are considerably less abundant than 'Fe-rich' cores (Mg# = 78.9–87.8; NiO = 0.03–0.34 wt%; MnO = 0.09–0.22 wt%; CaO < 0.10 wt%; $n = 15$). As for the Limpeza-18 and Samada Fe-rich cores, Mg# is positively correlated with NiO and inversely correlated with MnO (Fig. 11). There is significant overlap between the core compositions for the Samada and New Robinson grains. Olivine rims have

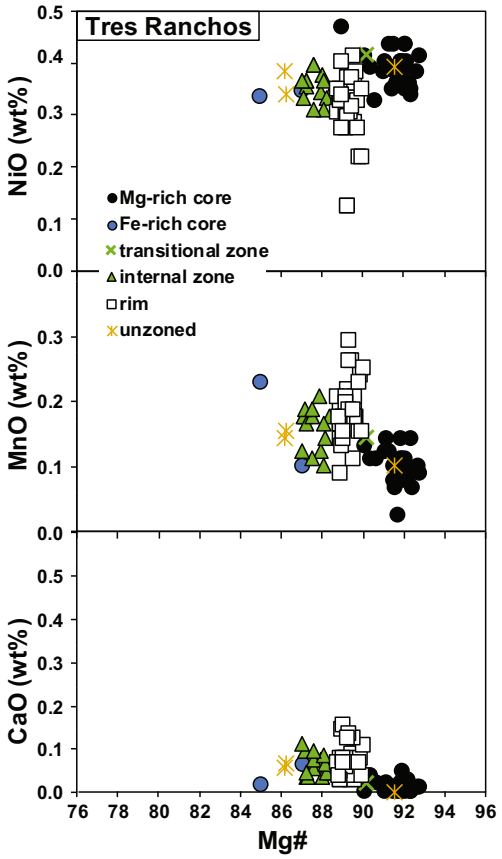

Fig. 9 Mg# vs NiO, MnO and CaO covariations charts of different zones in olivine grains from the Tres Ranchos-04 kimberlite, Alto Paranaiba Igneous Province, Brazil

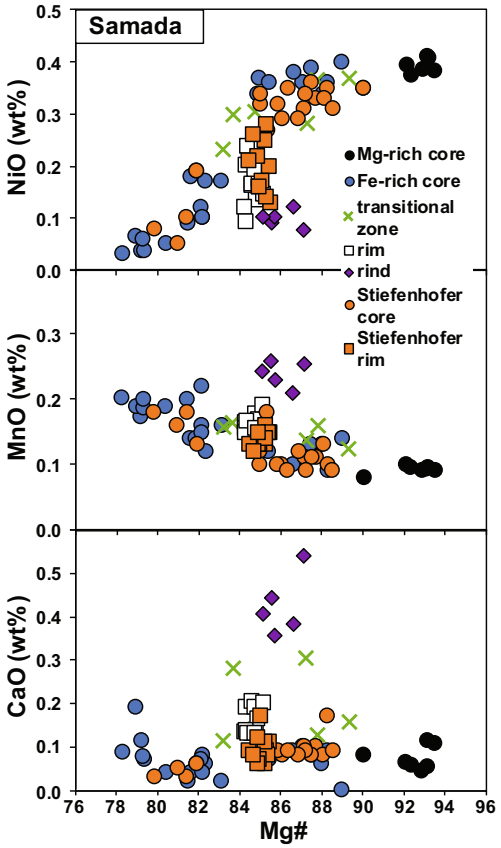

Fig. 10 Mg# vs NiO, MnO and CaO covariations charts of different zones in olivine grains from the Samada pipe, Kaalvallei kimberlite cluster, South Africa. 'Stiefenhofer cores' and 'Stiefenhofer rims' are analyses from Stiefenhofer (1989)

constant Mg# (82.7–83.9), but lower values than those of the Samada sample. Rim NiO contents decrease (0.21–0.02 wt%) with increasing MnO (0.14–0.24 wt%) and CaO concentrations (0.05–0.17 wt%). The transitional zones between cores and rims have Mg# values greater than the rims, consistent with their occurrence in contact with cores showing higher Mg# (see also Fig. 5c).

Discussion

The kimberlites investigated in this study are from different tectonic settings and exhibit a variety of textures (i.e. pyroclastic coherent vs hypabyssal kimberlites) and groundmass compositions (i.e. enrichment in carbonate or phlogopite plus oxide minerals). This comprehensive sample set allows comparison of olivine zoning in kimberlite magmas of variable composition and different emplacement mechanisms. In the following sections, we discuss the origin of the various olivine zones and implications for the evolution of kimberlite systems. We then address the relationships between olivine zoning and variations in texture and groundmass mineralogy.

Xenocrystic nature of olivine cores

'Mg-rich' olivine cores are characterised by Mg# values >89, high NiO (>0.22 wt%), variable MnO (0.04–0.19 wt%) and low CaO (<0.10 wt%) concentrations. These compositions overlap those of olivine in coarse-grained granular peridotites entrained in kimberlites worldwide (Fig. 12); including harzburgite and lherzolite xenoliths from the Ekati area (Menzies et al. 2004). This and the occurrence of lithospheric mantle phases included in these cores (e.g., Cr-diopside and Cr-spinel in the Koala grains) indicate core derivation from disaggregated mantle peridotites. In detail, the Mg-rich cores in olivine from the Brazilian samples show more restricted compositions (i.e. Mg# <92.8; Figs. 8 and 9), consistent with previous olivine analyses for the APIP kimberlites (Araujo et al. 2001) and values for mantle xenoliths from the Tres Ranchos kimberlite cluster (Leonardos et al. 1993). The absence of olivine with higher Mg# composition (i.e. >93) in the Tres Ranchos-04 and Limpeza-18 kimberlites suggests either refertilisation of the underlying cratonic lithospheric mantle, or sampling limited to shallower off-craton mantle. The latter explanation seems unlikely given the association of diamonds with at least some kimberlites in the region (Read et al. 2004).

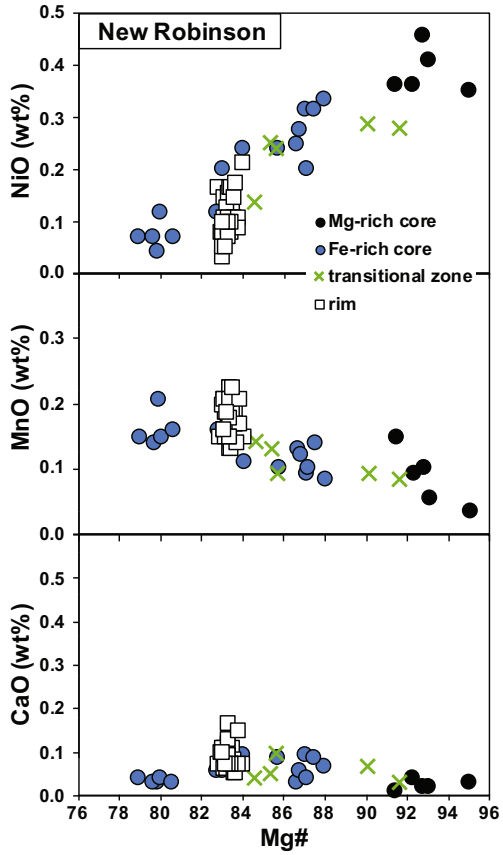

Fig. 11 Mg# vs NiO, MnO and CaO covariations charts of different zones in olivine grains from the New Robinson pipe, Kaalvallei kimberlite cluster, South Africa

Refertilisation of the underlying cratonic mantle is supported by the composition of clinopyroxene xenocrysts from kimberlites and kamafugites in the area, which record a progressive enrichment and thinning of the lithospheric mantle during the Cretaceous (Grütter 2009; Read et al. 2004).

'Fe-rich' olivine cores show Mg# <89–90, decreasing Mg# and NiO (0.40 to 0.03 wt%), increasing MnO (0.09 to 0.23 wt%) and variable CaO concentrations (<0.19 wt%). The contrasting geochemical trends exhibited by 'Mg-rich 'and 'Fe-rich' olivine probably indicate different origins. The compositions of 'Fe-rich' cores are similar to those of southern African kimberlitic megacrysts (Boyd and Nixon 1975; Gurney et al. 1979; Hops et al. 1992) and olivine in sheared peridotites from worldwide localities (Fig. 12), which suggests a genetic link. 'Fe-rich' olivine cores constitute a substantial proportion of the Kaalvallei and Limpeza-18 samples, represent a minor component of the Tres Ranchos-04 and Koala samples, and are absent from Grizzly. Other kimberlites that host significant amounts of olivine grains with 'Fe-rich' core compositions include Monastery in the Kaapvaal craton (Moore 1988) and Colossus in the Zimbabwe craton (Moore and Costin 2016). There is therefore no apparent relationship between the abundance of 'Fe-rich' cores and tectonic setting (craton margins vs interiors) or location (Sao Francisco, Kaapvaal and Zimbabwe cratons). However, it is important to note that 'Fe-rich' olivine cores are rare in the Lac de Gras kimberlites (this study; Brett et al. 2009; Bussweiler et al. 2015; Fedortchouk and Canil 2004).

In accord with several previous studies (Arndt et al. 2010; Brett et al. 2009; Bussweiler et al. 2015; Fedortchouk and Canil 2004; Giuliani and Foley 2016; Giuliani et al. 2017; Howarth and Taylor 2016; Kamenetsky et al. 2008; Nielsen and Sand 2008; Pilbeam et al. 2013; Sazonova et al. 2015; Shaikh et al. 2018; Sobolev et al. 2015), the current data indicate that olivine cores in kimberlites worldwide originate from different types of disaggregated mantle rocks (i.e. peridotite xenoliths and megacrysts), which occur in variable proportions in different kimberlites. A xenocrystic origin is consistent with rounded shapes and embayments shown by many cores (e.g., Figs. 3d, e), which is consistent with chemical resorption, potentially combined with some mechanical abrasion (Brett et al. 2015; Jones et al. 2014). Our data do not preclude the possibility that some olivine cores could originate from recently metasomatised peridotites (Howarth and Taylor 2016; Sazonova et al. 2015; Sobolev et al. 2015) and 'defertilised' dunites (Arndt et al. 2010). In fact, kimberlitic megacrysts and sheared peridotites are widely believed to be related to kimberlite metasomatism in the lithospheric mantle (Kargin et al. 2017; Kopylova et al. 2009; Moore and Belousova 2005; Moore and Lock 2001; Nowell et al. 2004; Pivin et al. 2013; Tappe et al. 2011; Woodhead et al. 2017).

Formation of transitional zones

The transitional zones documented in many olivine grains appear as diffuse layers (Figs. 3 and 5c, d) with compositions intermediate between those of cores and rims, but no clear compositional trends, even in samples where multiple transitional zones were examined (e.g., New Robinson; Fig. 11). Similar transitional zones have been documented from the Kangamiut aillikite/kimberlite rocks (Greenland) by Cordier et al. (2015), and Benfontein kimberlite sills (Kimberley, South Africa) by Howarth and Taylor (2016). These zones could result from partial re-equilibration of olivine cores in the ascending kimberlite before olivine supersaturation and rim overgrowth (Howarth and Taylor 2016). In addition, the diffuse character of the transitional zones (Figs. 5c, d and S2) suggests a contribution from diffusive exchange between cores and rims.

This study shows that transitional zones represent a ubiquitous feature of olivine grains in kimberlites due to disequilibrium of xenocrystic cores in kimberlite magmas. Identification of these zones in BSE images depends on the compositional contrast between core and rim as well as core residence times, and therefore depth of entrainment, in kimberlite magmas.

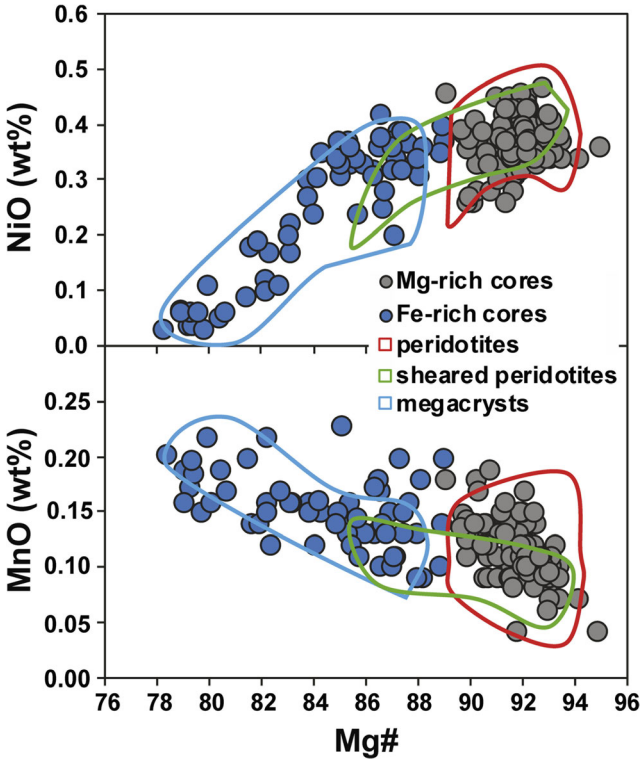

Fig. 12 Mg# vs (**a**) NiO and (**b**) MnO covariation charts comparing the compositions of 'Mg-rich' and 'Fe-rich' olivine cores measured in this study to analyses of coarse-grained granular 'peridotites' and 'sheared peridotites' from worldwide localities, and olivine 'megacrysts' from southern African kimberlites

Significance of internal zones

Internal zones have been observed in some grains from Grizzly (4; Fig. 3a), Limpeza-18 (5; Fig. 3c) and Tres Ranchos-04 (14; Figs. 3d and 5a, b). In all three kimberlites, internal zones exhibit relatively restricted Mg# values that are lower than those of associated rims at broadly similar NiO and MnO concentrations (Figs. 6, 8, 9). These features, combined with evidence of resorption (i.e. embayments; e.g., Fig. 5a), suggest these internal zones may have crystallised from early pulses of evolved kimberlite melt at mantle depths before entrainment in the ascending kimberlite magma. The low Ca contents could be explained by concurrent crystallisation of (or equilibration with) clinopyroxene, which is stable in kimberlite-like silicate-carbonate melts at mantle depths (e.g., Luth 2009; Stone and Luth 2016). This interpretation of the formation of internal zones is consistent with abundant evidence of kimberlite metasomatism in the mantle coeval with, or just preceding kimberlite emplacement (Bussweiler et al. 2016; Dawson et al. 2001; Fitzapyne et al. 2018; Giuliani et al. 2013, 2014, 2016; Kamenetsky et al. 2014a; Kargin et al. 2016; Lawless et al. 1979; Jollands et al. 2018; Soltys et al. 2016).

Conversely, internal zones in olivine from the De Beers kimberlite show euhedral shapes (Soltys et al. 2018b). Similar euhedral internal zones were also reported by Howarth and Taylor (2016, their Fig. 4a, b) for the Benfontein kimberlite. The compositions of internal zones in olivine from De Beers and Benfontein cluster at higher Mg# and Ni contents than those of their respective rims. As suggested by Soltys et al. (2018b), those internal zones probably represent the early crystallisation product of the ascending kimberlite, which is consistent with inclusions of (magmatic) chromite. The occurrence of distinct types of olivine internal zones in different kimberlites (i.e. this study vs Soltys et al. 2018b), and their absence in others (e.g., Kaalvallei), underlines the complex and non-unique evolution of kimberlite systems at each locality.

Magmatic crystallisation of rims and rinds

The characteristic features of olivine rims (i.e. relatively constant Mg# (<2 units) at decreasing Ni and increasing Mn and Ca contents), combined with the occurrence of inclusions of groundmass minerals (e.g., spinel but also phlogopite, apatite and perovskite; see Limpeza-18 olivine), clearly show that the rims crystallised from kimberlite magmas at and/or just before emplacement (see also Arndt et al. 2010; Brett et al. 2009; Bussweiler et al. 2015; Fedortchouk and Canil 2004; Giuliani 2018; Giuliani et al. 2017; Howarth and Taylor 2016; Kamenetsky et al. 2008; Nielsen and Sand 2008; Pilbeam et al. 2013; Sazonova et al. 2015; Sobolev et al. 2015; Soltys et al. 2018b). The differences in average Mg# composition of olivine rims from different kimberlites probably reflect differences in parental melt compositions (see below).

Although the olivine rims of each kimberlite form subvertical arrays in Mg# vs Ni, Mn, Ca covariation plots, some sloping trends can be observed. A decrease of Mg# (83.9 to 82.9 at decreasing NiO (0.21 to 0.02 wt%) is observed at New Robinson (Fig. 11), but also at Bultfontein (Giuliani et al. 2017). Rims of Koala olivine are characterised by increasing MnO (0.10 to 0.20 wt%) at decreasing Mg# (92.2 to 90.8), with two higher-MnO analyses plotting out of this trend (Fig. 7). Conversely, a concomitant decrease of Mg# and MnO is apparent in Tres Ranchos-04 olivine rims (Fig. 9), while Soltys et al. (2018b) report a negative relationship between Mg# and NiO concentrations for De Beers olivine rims. In summary, there seems to be no consistent evolution path in the compositions of olivine rims examined in this and previous studies. Localised conditions including oxygen fugacity variations, fractionation of magmatic phases (e.g., spinel, ilmenite) and assimilation of entrained material probably affect kimberlite melt compositions in different ways both at the local and global scale. Large changes in Ni concentrations at relatively constant Mg# might be due to elevated values of Ni partitioning between olivine and kimberlite melts (Cordier et al. 2015).

The rinds that fringe the rims of olivine grains in some kimberlites host inclusions of calcite and phlogopite (see Koala

olivine), suggesting formation late in the magmatic evolution of kimberlites. The compositional features (i.e. increasing Mg#, Mn and Ca at decreasing Ni contents) of the rinds examined in this and previous studies (e.g., Figs. 7 and 10) have been used as evidence to support various formation mechanisms, including equilibration with late-stage carbonatitic fluids (Pilbeam et al. 2013), and crystallisation from residual kimberlite melts at high oxygen fugacity conditions (Bussweiler et al. 2015; Fedortchouk and Canil 2004; Howarth and Taylor 2016). The latter interpretation is consistent with spinel evolution to MUM spinel and then Ti-magnetite (i.e. high Fe^{3+}/Fe^{2+}) compositions in kimberlites worldwide, as well as the presence of olivine rinds in the carbonate-poor Samada kimberlite sample (Supplementary Fig. S1). Koala olivine rinds differ from those examined in other kimberlites, because several discrete zones are present (Fig. 3b; see also Kamenetsky et al. 2013). The apparent oscillatory zoning noticeable in Fig. 3b coincides with a progressive increase in Mg# (Fig. 7). and could be due to rapid, non-equilibrium crystallisation conditions (e.g., Shore and Fowler 1996).

Relationship between olivine composition, kimberlite texture and groundmass mineralogy

Olivine rims in the examined kimberlites show variable average Mg# composition of between ~83.3 (New Robinson) and 91.5 (Grizzly and Koala), which indicates different parental melt compositions. The Grizzly and Koala samples, which occur in close proximity within the Ekati area, exhibit different textural features (i.e. extent of olivine breakage; Fig. 2), due to moderately explosive and non-explosive magma emplacement, respectively. The compositions of their rims are however indistinguishable in terms of average Mg# (Grizzly: 91.5 ± 0.2; Koala: 91.5 ± 0.3, 1 s.d.). Koala olivine has developed thick rinds, whereas rinds are thin and scarce in Grizzly olivine. While examination of more pyroclastic and hypabyssal kimberlites samples from the same pipe or cluster will be required to confirm these observations, it is apparent that the emplacement style does not influence olivine rim compositions, whereas rinds might develop more extensively in hypabyssal kimberlites. A corollary is that the composition of the parental kimberlite magma, as shown by olivine rims, has little influence on the emplacement style of these kimberlites.

The samples examined in this study show very different proportions of groundmass components, i.e. dominant carbonates and (pseudomorphed) monticellite (~60–70 vol%; Table 1) in the Ekati kimberlites; abundant (≥30 vol%) phlogopite and oxide minerals (spinel, Mg-ilmenite, perovskite; e.g., Fig. 1e, f) in the Brazilian and Kaalvallei kimberlites. Our results show a robust inverse correlation between groundmass mineralogy (i.e. vol% of phlogopite plus oxide phases) and olivine rim compositions (i.e. average Mg#; Fig. 13). This correlation can probably be extended to other carbonate-rich kimberlites worldwide including Diavik and Leslie in the Lac de Gras field (e.g., Moss et al. 2009), and Udachnaya-East in Siberia (e.g., Kamenetsky et al. 2014b), where olivine rims show elevated Mg# (~89–91; Bussweiler et al. 2015; Brett et al. 2009; Kamenetsky et al. 2008). It is therefore apparent that kimberlite magmas more enriched in Fe generate olivine with lower Mg# and crystallise higher proportions of phlogopite and Fe-bearing oxide minerals in the groundmass.

Conclusions

This study demonstrates that olivine in kimberlites from different continents and tectonic settings have broadly similar zoning patterns characterised by xenocrystic core, magmatic rim, transitional zone between core and rim, and, when preserved, (magmatic) rind. Transitional zones result from partial re-equilibration of xenocrystic cores with the entraining kimberlite combined with diffusive exchange between cores and rims. An additional internal zone is present in olivine from some kimberlites and probably reflects early kimberlite activity in the mantle.

Despite this similarity, the compositions of each olivine zone show significant variations in kimberlites worldwide. The proportions of cores derived from granular peridotites and kimberlite-metasomatised mantle (i.e. sheared peridotites and megacrysts) vary largely between localities, but are unrelated to tectonic setting. The compositions of magmatic rims show marginally different Mg# vs Ni, Mn, Ca trends, which suggest variable influence of different factors including

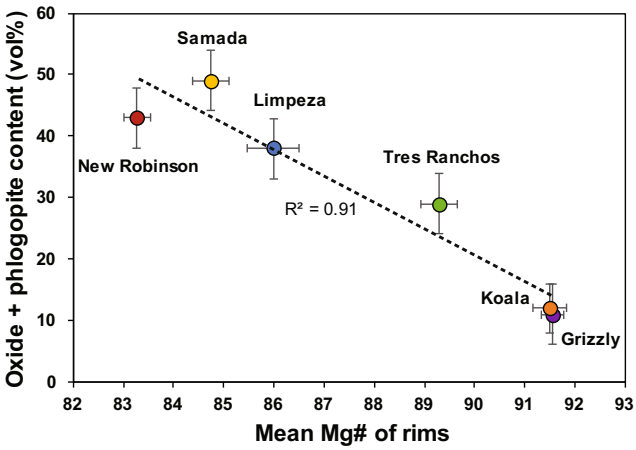

Fig. 13 Diagram comparing the mean (±1.s.d.) Mg# value of olivine rims with the estimated abundance of phlogopite plus oxide minerals (spinel + Mg-ilmenite + perovskite) in the groundmass of kimberlites examined in this study. Note the statistical robustness of the inverse correlation between the two parameters ($R^2 = 0.91$). An arbitrary uncertainty of ±5% is applied to mineral modal abundances to account for variations within examined thin sections

oxygen fugacity, fractionation of magmatic phases and assimilation of entrained material. In each kimberlite, olivine rims exhibit a restricted range of Mg# values, which however varies significantly between localities (i.e. from ~91.5 at Ekati to ~83.3 at New Robinson). Average Mg# values of olivine rims are inversely correlated to the abundance of phlogopite plus oxide phases in the groundmass, which provides robust evidence for a direct correlation between olivine rim composition, groundmass mineralogy and, therefore, melt composition. Conversely, the composition of olivine in nearby kimberlites that show explosive (Grizzly) and hypabyssal emplacement (Koala) is remarkably similar, except for thicker and more abundant rinds in Koala.

In summary, olivine commonly shows very complex zoning patterns in kimberlites from worldwide localities, which provides invaluable insights into the evolution of kimberlite systems from early kimberlite metasomatism at mantle depths to late crystallisation of residual kimberlite melts after emplacement. The unique zoning of olivine in kimberlites is potentially a diagnostic feature of kimberlite rocks.

Acknowledgements We acknowledge provision of samples from the Ekati mine by BHP Billiton, and permission obtained from Dominion Diamond Mines ULC to publish our results. Samples from Limpeza-18, Tres Ranchos-04, and Samada were generously provided by the De Beers Group, while the New Robinson kimberlite was sourced in the John J. Gurney Upper Mantle Room Collection housed at the University of Cape Town. We would like to thank Graham Hutchinson for his aid with SEM and EPMA analyses at the University of Melbourne. Thoughtful reviews by Nick Arndt and Curtis Brett and the editorial handling by Phil Janney and Lutz Nasdala improved the final manuscript. This research was supported by the Australian Research Council through a Discovery Early Career Research Award (DECRA) to AG (grant n. DE-150100009). This is publication 32 from the Kimberlites and Diamonds Research Group at the University of Melbourne, also listed as contribution 1173 from the ARC Centre of Excellence for Core to Crust Fluid Systems and 1234 from the GEMOC Key Centre.

References

Araujo A, Carlson RW, Gaspar JC, Bizzi LA (2001) Petrology of kamafugites and kimberlites from the Alto Paranaíba Alkaline Province, Minas Gerais, Brazil. Contrib Mineral Petr 142(2):163–177

Armstrong JP, Wilson M, Barnett RL, Nowicki T, Kjarsgaard BA (2004) Mineralogy of primary carbonate-bearing hypabyssal kimberlite, Lac de Gras, Slave Province, Northwest Territories, Canada. Lithos 76(1–4):415–433

Arndt NT, Guitreau M, Boullier AM, le Roex A, Tommasi A, Cordier P, Sobolev A (2010) Olivine, and the origin of kimberlite. J Petrol 51(3):573–602

Boyd FR, Nixon PH (1975) Origins of the ultramafic nodules from some kimberlites of northern Lesotho and the Monastery Mine, South Africa. Phys Chem Earth 9:431–454

Brett RC, Russell JK, Moss S (2009) Origin of olivine in kimberlite: phenocryst or impostor? Lithos 112:201–212

Brett RC, Russell JK, Andrews GDM, Jones TJ (2015) The ascent of kimberlite: insights from olivine. Earth Planet Sc Lett 424:119–131

Bussweiler Y, Foley SF, Prelević D, Jacob DE (2015) The olivine macrocryst problem: new insights from minor and trace element compositions of olivine from Lac de Gras kimberlites, Canada. Lithos 220–223:238–252

Bussweiler Y, Stone R, Pearson D, Luth R, Stachel T, Kjarsgaard B, Menzies A (2016) The evolution of calcite-bearing kimberlites by melt-rock reaction: evidence from polymineralic inclusions within clinopyroxene and garnet megacrysts from Lac de Gras kimberlites, Canada. Contrib Mineral Petr 171(7):1–25

Canil D, Fedortchouk Y (1999) Garnet dissolution and the emplacement of kimberlites. Earth Planet Sc Lett 167(3–4):227–237

Cordier C, Sauzeat L, Arndt NT, Boullier A-M, Batanova V, Barou F (2015) Metasomatism of the lithospheric mantle immediately precedes kimberlite eruption: new evidence from olivine composition and microstructures. J Petrol 56(9):1775–1796

Dawson J, Hill P, Kinny P (2001) Mineral chemistry of a zircon-bearing, composite, veined and metasomatised upper-mantle peridotite xenolith from kimberlite. Contrib Mineral Petr 140(6):720–733

Downes PJ, Wartho J-A, Griffin BJ (2006) Magmatic evolution and ascent history of the aries micaceous kimberlite, Central Kimberley basin, Western Australia: evidence from zoned phlogopite phenocrysts, and UV laser $^{40}Ar/^{39}Ar$ analysis of phlogopite-biotite. J Petrol 47(9):1751–1783

Fedortchouk Y, Canil D (2004) Intensive variables in kimberlite magmas, Lac de Gras, Canada and implications for diamond survival. J Petrol 45(9):1725–1745

Felgate MR (2014) The petrogenesis of Brazilian kimberlites and kamafugites intruded along the 125° lineament: improved geochemical and geochronological constraints on magmatism in Rondonia and the Alto Paranaiba Igneous Province. PhD thesis, The University of Melbourne, Australia

Fitzapyne A, Giuliani A, Phillips D, Hergt J, Woodhead JD, Farquhar J, Fiorentini ML, Drysdale RN, WU N (2018) Kimberlite-related metasomatism recorded in MARID and PIC mantle xenoliths. Miner Petrol, this volume

Gibson S, Thompson R, Leonardos O, Dickin A, Mitchell J (1995) The Late Cretaceous impact of the Trindade mantle plume: evidence from large-volume, mafic, potassic magmatism in SE Brazil. J Petrol 36(1):189–229

Giuliani A (2018) Insights into kimberlite petrogenesis and mantle metasomatism from a review of the compositional zoning of olivine in kimberlites worldwide. Lithos 312-313:322–342

Giuliani A, Foley SF (2016) The geochemical complexity of kimberlite rocks and their olivine populations: a comment on cordier et al. (Journal of Petrology, 56, 1775–1796, 2015). J Petrol 57(5):921–926

Giuliani A, Kamenetsky VS, Kendrick MA, Phillips D, Wyatt BA, Maas R (2013) Oxide, sulphide and carbonate minerals in a mantle polymict breccia: Metasomatism by proto-kimberlite magmas, and relationship to the kimberlite megacrystic suite. Chem Geol 353:4–18

Giuliani A, Phillips D, Kamenetsky VS, Kendrick MA, Wyatt BA, Goemann K, Hutchinson G (2014) Petrogenesis of mantle polymict breccias: insights into mantle processes coeval with kimberlite magmatism. J Petrol 55(4):831–858

Giuliani A, Phillips D, Kamenetsky VS, Goemann K (2016) Constraints on kimberlite ascent mechanisms revealed by phlogopite compositions in kimberlites and mantle xenoliths. Lithos 240–243:189–201

Giuliani A, Soltys A, Phillips D, Kamenetsky VS, Maas R, Goemann K, Woodhead JD, Drysdale RN, Griffin WL (2017) The final stages of kimberlite petrogenesis: petrography, mineral chemistry, melt inclusions and Sr-C-O isotope geochemistry of the Bultfontein kimberlite (Kimberley, South Africa). Chem Geol 455:342–356

Grütter HS (2009) Pyroxene xenocryst geotherms: techniques and application. Lithos 112(Supplement 2):1167–1178

Guarino V, Wu F-Y, Lustrino M, Melluso L, Brotzu P, Gomes CB, Ruberti E, Tassinari CCG, Svisero DP (2013) U–Pb ages, Sr–Nd-

isotope geochemistry, and petrogenesis of kimberlites, kamafugites and phlogopite-picrites of the Alto Paranaíba Igneous Province, Brazil. Chem Geol 353:65–82

Gurney JJ, Jakob WRO, Dawson JB (1979) Megacrysts from the Monastery kimberlite pipe. In: Boyd FR, Meyer HOA (eds) The Mantle Sample. Proceedings of the 2nd International Kimberlte Conference. American Geophysical Union, Washington, DC, pp 227–243

Hops JJ, Gurney JJ, Harte B (1992) The jagersfontein Cr-poor megacryst suite: towards a model for megacryst petrogenesis. J Volcanol Geoth Res 50(1–2):143–160

Howarth GH, Taylor LA (2016) Multi-stage kimberlite evolution tracked in zoned olivine from the Benfontein sill, South Africa. Lithos 262: 384–397

Hunter RH, Taylor LA (1982) Instability of garnet from the mantle: glass as evidence of metasomatic melting. Geology 10(12):617–620

Jollands MC, Hanger BJ, Yaxley GM, Hermann J, Kilburn MR (2018) Timescales between mantle metasomatism and kimberlite ascent indicated by diffusion profiles in garnet crystals from peridotite xenoliths. Earth Planet Sc Lett 481:143–153

Jones TJ, Russell JK, Porritt LA, Brown RJ (2014) Morphology and surface features of olivine in kimberlite: implications for ascent processes. Solid Earth 5(1):313–326

Kamenetsky VS, Kamenetsky MB, Sobolev AV, Golovin AV, Demouchy S, Faure K, Sharygin VV, Kuzmin DV (2008) Olivine in the Udachnaya-East kimberlite (Yakutia, Russia): types, compositions and origins. J Petrol 49(4):823–839

Kamenetsky VS, Kamenetsky MB, Sobolev AV, Golovin AV, Sharygin VV, Pokhilenko NP, Sobolev NV (2009) Can pyroxenes be liquidus minerals in the kimberlite magma? Lithos 112S:213–222

Kamenetsky VS, Grutter H, Kamenetsky MB, Goemann K (2013) Parental carbonatitic melt of the Koala kimberlite (Canada): constraints from melt inclusions in olivine and Cr-spinel, and groundmass carbonate. Chem Geol 353:96–111

Kamenetsky VS, Belousova EA, Giuliani A, Kamenetsky MB, Goemann K, Griffin WL (2014a) Chemical abrasion of zircon and ilmenite megacrysts in the Monastery kimberlite: implications for the composition of kimberlite melts. Chem Geol 383:76–85

Kamenetsky VS, Golovin AV, Maas R, Giuliani A, Kamenetsky MB, Weiss Y (2014b) Towards a new model for kimberlite petrogenesis: evidence from unaltered kimberlites and mantle minerals. Earth-Sci Rev 139:145–167

Kargin AV, Sazonova LV, Nosova AA, Tretyachenko VV (2016) Composition of garnet and clinopyroxene in peridotite xenoliths from the Grib kimberlite pipe, Arkhangelsk diamond province, Russia: evidence for mantle metasomatism associated with kimberlite melts. Lithos 262:442–455

Kargin AV, Sazonova LV, Nosova AA, Lebedeva NM, Tretyachenko VV, Abersteiner A (2017) Cr-rich clinopyroxene megacrysts from the Grib kimberlite, Arkhangelsk province, Russia: relation to clinopyroxene–phlogopite xenoliths and evidence for mantle metasomatism by kimberlite melts. Lithos 292-293:34–48

Kopylova MG, Nowell GM, Pearson DG, Markovic G (2009) Crystallization of megacrysts from protokimberlitic fluids: geochemical evidence from high-Cr megacrysts in the Jericho kimberlite. Lithos 112S:284–295

Lawless PJ, Gurney JJ, Dawson JB (1979) Polymict peridotites from the Bultfontein and De Beers mines, Kimberley, South Africa. In: Boyd FR, Meyer HOA (eds) The Mantle Sample. Proceedings of the 2nd International Kimberlte Conference. American Geophysical Union, Washington, DC, pp 145–155

Leonardos OH, Carvalho JB, Tallarico FHB, Gibson SA, Thompson RN, Meyer HOA, Dickin AP (1993) O xenolito de granada Iherzolito de Tres Ranches 4: uma rocha matriz do diamante na provfncia magmatica cretacea do Alto Paranaíba. Annais de Simpósio de Geologia do Diamanteo. Unversidade Federal do Mato Grosso. Special Publication 1:3–16

Luth RW (2009) The activity of silica in kimberlites, revisited. Contrib Mineral Petr 158(2):283–294

Menzies A, Westerlund K, Grütter H, Gurney J, Carlson J, Fung A, Nowicki T (2004) Peridotitic mantle xenoliths from kimberlites on the Ekati Diamond Mine property, N.W.T., Canada: major element compositions and implications for the lithosphere beneath the central Slave craton. Lithos 77(1–4):395–412

Mitchell RH (2008) Petrology of hypabyssal kimberlites: relevance to primary magma compositions. J Volcanol Geotherm Res 174(1–3): 1–8

Moore AE (1988) Olivine: a monitor of magma evolutionary paths in kimberlites and olivine melilitites. Contrib Mineral Petr 99(2): 238–248

Moore A, Belousova E (2005) Crystallization of Cr-poor and Cr-rich megacryst suites from the host kimberlite magma: implications for mantle structure and the generation of kimberlite magmas. Contrib Mineral Petr 149(4):462–481

Moore A, Costin G (2016) Kimberlitic olivines derived from the Cr-poor and Cr-rich megacryst suites. Lithos 258:215–227

Moore AE, Lock NP (2001) The origin of mantle-derived megacrysts and sheared peridotites-evidence from kimberlites in the northern Lesotho-Orange Free State (South Africa) and Botswana pipe clusters. S Afr J Geol 104(1):23–38

Moss S, Russell JK, Brett RC, Andrews GDM (2009) Spatial and temporal evolution of kimberlite magma at A154N, Diavik, Northwest Territories, Canada. Lithos 112S:541–552

Moss S, Russell JK, Smith BHS, Brett RC (2010) Olivine crystal size distributions in kimberlite. Am Mineral 95(4):527–536

Nielsen TFD, Sand KK (2008) The Majuagaa kimberlite dike, Maniitsoq region, western Greenland: constraints on an Mg-rich silicocarbonatitic melt composition from groundmass mineralogy and bulk compositions. Can Mineral 46(4):1043–1061

Nowell GM, Pearson DG, Bell DR, Carlson RW, Smith CB, Kempton PD, Noble SR (2004) Hf isotope systematics of kimberlites and their megacrysts: new constraints on their source regions. J Petrol 45(8): 1583–1612

Nowicki T, Crawford B, Dyck D, Carlson J, McElroy R, Oshust P, Helmstaedt H (2004) The geology of kimberlite pipes of the Ekati property, Northwest Territories, Canada. Lithos 76(1–4):1–27

Nowicki T, Porritt L, Crawford B, Kjarsgaard B (2008) Geochemical trends in kimberlites of the Ekati property, Northwest Territories, Canada: insights on volcanic and resedimentation processes. J Volcanol Geotherm Res 174(1–3):117–127

Pilbeam LH, Nielsen TFD, Waight TE (2013) Digestion fractional crystallization (DFC): an important process in the genesis of kimberlites: evidence from olivine in the Majuagaa kimberlite, southern West Greenland. J Petrol 54(7):1399–1425

Pivin M, Debaille V, Mattielli N, Demaiffe D (2013) Nd–Hf isotope systematics of megacrysts from the Mbuji-Mayi kimberlites, D. R. Congo: evidence for a metasomatic origin related to kimberlite interaction with the cratonic lithospheric mantle. In: Pearson GD, Grütter SH, Harris WJ, Kjarsgaard AB, O'Brien H, Rao CNV, Sparks S (eds) Proceedings of the 10th International Kimberlite Conference. Springer, New Delhi, pp 123–136

Porritt LA, Cas RA (2011) The influence of complex intra-and extra-vent processes on facies characteristics of the Koala Kimberlite, NWT, Canada: volcanology, sedimentology and intrusive processes. Bull Volcanol 73(6):717–735

Read G, Grutter H, Winter S, Luckman N, Gaunt F, Thomsen F (2004) Stratigraphic relations, kimberlite emplacement and lithospheric thermal evolution, Quiricó Basin, Minas Gerais State, Brazil. Lithos 77(1):803–818

Russell JK, Porritt LA, Lavallee Y, Dingwell DB (2012) Kimberlite ascent by assimilation-fuelled buoyancy. Nature 481(7381):352–356

Sazonova LV, Nosova AA, Kargin AV, Borisovskiy SE, Tretyachenko VV, Abazova ZM, Griban' YG (2015) Olivine from the Pionerskaya and V. Grib kimberlite pipes, Arkhangelsk diamond province, Russia: types, composition, and origin. Petrology 23(3):227–258

Shaikh AM, Kumar SP, Patel SC, Thakur SS, Ravi S, Behera D (2018) The P3 kimberlite and P4 lamproite, Wajrakarur kimberlite field, India: mineralogy, and major and minor element compositions of olivines as records of their phenocrystic vs xenocrystic origin. Miner Petrol, this volume

Shore M, Fowler AD (1996) Oscillatory zoning in minerals; a common phenomenon. Can Mineral 34(6):1111–1126

Sobolev NV, Sobolev AV, Tomilenko AA, Kovyazin SV, Batanova VG, Kuz'min DV (2015) Paragenesis and complex zoning of olivine macrocrysts from unaltered kimberlite of the Udachnaya-East pipe, Yakutia: relationship with the kimberlite formation conditions and evolution. Russ Geol Geophys 56(1–2):260–279

Soltys A, Giuliani A, Phillips D, Kamenetsky VS, Maas R, Woodhead J, Rodemann T (2016) In-situ assimilation of mantle minerals by kimberlitic magmas – direct evidence from a garnet wehrlite xenolith entrained in the Bultfontein kimberlite (Kimberley, South Africa). Lithos 256:182–196

Soltys A, Giuliani A, Phillips D (2018a) A new approach to reconstructing the composition and evolution of kimberlite melts: a case study of the archetypal Bultfontein kimberlite (Kimberley, South Africa). Lithos 304–307:1–15

Soltys A, Giuliani A, Phillips D (2018b) Crystallisation and melt evolution of the De Beers dyke (Kimberley, South Africa). Miner Petrol, this volume

Stiefenhofer J (1989) Petrography, mineralogy and geochemistry of the Kaalvallei kimberlite pipe. Rhodes University, Grahamstown, South Africa, Orange Free State. B Sc Hons Thesis

Stone RS, Luth RW (2016) Orthopyroxene survival in deep carbonatite melts: implications for kimberlites. Contrib Mineral Petr 171(7):1–9

Tappe S, Pearson DG, Nowell G, Nielsen T, Milstead P, Muehlenbachs K (2011) A fresh isotopic look at Greenland kimberlites: Cratonic mantle lithosphere imprint on deep source signal. Earth Planet Sc Lett 305(1–2):235–248

Taylor WR, Kingdom L (1999) Mineralogy of the Jagersfontein kimberlite - an unusual Group I micaceous kimberlite - and a comment on the robustness of the mineralogical definition of 'orangeite'. In: Gurney JJ, Gurney JL, Pascoe MD, Richardson SH (eds) 7th Intern Kimb Conf, vol 2. Red Roof Design, Cape Town, pp 861–866

Webb KJ, Crawford B, Nowicki TE, Hetman CM, Carlson J (2008) Coherent kimberlite at Ekati, Northwestern Territories, Canada: textural and geochemical variations and implications for emplacement. 9th Intern Kimb Conf. In: Ext Abstr 9IKC-A-00225

Woodhead J, Hergt J, Giuliani A, Phillips D, Maas R (2017) Tracking continental-scale modification of the Earth's mantle using zircon megacrysts. Geochem Persp Lett 4:1–6